Ultrashort laser pulses and ultrashort electron bunches generated in relativistic laser-plasma interaction[a)]

J. Faure[b)] and Y. Glinec
Laboratoire d'Optique Appliquée, École Polytechnique, ENSTA, CNRS, UMR 7639, Palaiseau, France

G. Gallot
Laboratoire d'Optique et Biosciences, CNRS UMR 7645-INSERM U696-Ecole Polytechnique-ENSTA, Palaiseau, France

V. Malka
Laboratoire d'Optique Appliquée, École Polytechnique, ENSTA, CNRS, UMR 7639, Palaiseau, France

(Received 24 October 2005; accepted 6 February 2006; published online 11 May 2006)

An experimental study of the interaction of ultrashort laser pulses with underdense plasmas in the relativistic regime is presented. A parameter regime of particular interest was found: the so-called bubble regime. In this regime, the laser pulse is focused to relativistic intensities and its pulse duration is comparable to or shorter than the plasma period. A wealth of physical phenomena occurs for such physical parameters. These phenomena have multiple signatures which have been investigated experimentally: (i) the generation of a high quality electron beam (high energy, very collimated, quasimonoenergetic energy distribution); (ii) the laser pulse temporal shortening in nonlinear plasma waves. In addition, experimental results suggest that the electron beam produced in this way has temporal structures shorter than 50 fs. © *2006 American Institute of Physics*.
[DOI: 10.1063/1.2180727]

I. INTRODUCTION

Electron beams can be generated from the interaction of ultraintense and ultrashort laser pulses with underdense plasmas.[1,2] The motivation for studying and developing these laser-plasma electron accelerators is dual: first, plasmas are able to sustain extremely high electric fields (on the order of 1 TeV/m) and as such, they can be used as accelerating structures for compact particle accelerators. Second, the interaction of ultrashort laser pulses with plasmas can, under certain conditions, generate ultrashort electron bunches. Simulations indicate that sub-100 fs electron bunch could be produced in this manner. Such ultrashort electron bunches can contribute to the progress of ultrafast science in fields as diverse as femto-chemistry,[3–5] the generation of femtosecond x-ray beams[6] for x-ray diffraction[7] for instance.

The first electron beams from laser-plasma interaction were obtained in the last decade.[1] In these early experiments, the so-called self-modulated laser wake field (SMLWF) regime[8–10] led to the generation of an electron beam. In the SMLWF, the laser pulse is longer than the plasma wavelength ($\tau c \gg \lambda_p$); under the action of the forward Raman instability or the self-modulation instability, the laser pulse temporal profile modulates at λ_p, which causes the excitation of a large amplitude plasma wave. This large density perturbation is the source of an electric field which will be used in turn to accelerate electrons. Electrons are injected into the plasma wave through wave breaking:[11] as the plasma wave rises to high amplitudes, the laser pulse heats the plasma background electrons through various mechanisms (Raman backscattering, Raman side scattering, etc.). The combination of these two elements leads to the breaking of the plasma wave and to the trapping of massive amounts of plasma electrons which are then accelerated in the wave. Electron beams produced in this manner have very specific characteristics: (i) they have a Maxwellian energy distribution, with electron energies ranging from 0 to hundreds of mega-electron-volts; (ii) they tend to have large divergence angles. Such beams are difficult to use for some applications because they are difficult to transport and to focus. In addition, because the electron beam has a 100% energy spread, the electron bunch stretches as it propagates due to velocity dispersion. Thus, the advantage of generating short bunches is lost once the beam has propagated.

Recently, several experiments have shown a tremendous improvement in the quality of electron beams that can be produced in a laser-plasma accelerator.[12–14] These experiments produced high quality electron beams with small divergence angles (<10 mrad), quasimonoenergetic energy distribution (with energy spreads from 5% to 25%), and high energies (100 MeV). This progress was accomplished because these experiments were performed in a different regime: they used shorter pulses (30–50 fs) and longer interaction lengths (3–5 mm). The short duration of the pulses minimized the role of instabilities as well as heating of the plasma background electrons, thus permitting higher plasma wave amplitudes[15] to be reached. The long interaction length gave the pulse time to evolve. It also provided a longer acceleration distance for electrons.

In our experiment,[12,16] the laser pulse was almost resonant with the plasma wave: its transverse and longitudinal

[a)]Paper KI2 5, Bull. Am. Phys. Soc. **50**, 183 (2005).
[b)]Invited speaker. Electronic mail: jerome.faure@ensta.fr

dimensions were close to the plasma wavelength. The interaction of intense and resonant-like laser pulses with a plasma has been called the bubble regime.[17] Simulations have shown that this regime is very well suited for producing high quality electron beams: quasimonoenergetic and highly collimated electron beams have been obtained in simulations. The following scenario has been established from the simulations: first, a nonlinear plasma wave is excited directly by the laser pulse ponderomotive force. As the pulse propagates in the plasma, it self-focuses and undergoes longitudinal compression by plasma waves. This decreases the effective radius of the laser pulse as well as its duration, and increases the laser intensity by one order of magnitude. This compressed laser pulse is now resonant with the plasma wave and it drives a highly nonlinear wake field; the laser ponderomotive potential expels the plasma electrons radially and leaves a cavitated region behind (this is referred to as "cavitation" or "blowout"). In this regime, the three-dimensional structure of the wake field resembles a plasma bubble (hence the name bubble regime). As the electron density at the walls of the bubble becomes large, electrons are injected and accelerated inside the bubble. Injection occurs at the very back of the plasma bubble. This localized injection, in conjunction with mechanisms such as dephasing and self-bunching, results in the generation of a quasimonoenergetic beam.

Observing all these fine effects experimentally is very challenging, but this regime of interaction has some very specific signatures: (i) the laser pulse is compressed in time; (ii) electron bunches are quasimonoenergetic; (iii) electron bunches are ultrashort ($<\lambda_p$). In this paper we will focus on the measurement of these signatures. Section II will address the question of the laser pulse duration and show that the highest quality electron beams are obtained when the shortest and highest intensity pulses are used. In Sec. III, we will describe how the laser pulse is shortened after traveling through the plasma. Finally, Sec. IV will focus on transition radiation as a diagnostics for electron bunch duration. We will show experimental evidence of ultrashort temporal structures in the electron bunch.

II. INFLUENCE OF LASER PULSE DURATION ON ELECTRON BEAM GENERATION

In principle, the highest quality electron beams are obtained in the bubble regime, when the laser pulse spatial dimensions are on the order of or smaller than the plasma wavelength. In this case, the accelerated electrons stay behind the laser pulse and the laser electric field does not disturb them. It is likely that in the case of a longer pulse, the laser electric field scatters electrons in the phase space, thus destroying the well-defined peaks of the energy distribution and also increasing the divergence angle of the beam. In order to check this point, we performed an experiment where the pulse duration was varied with respect to the plasma wavelength.

A. Experimental setup

The experiment was performed using an ultraintense laser pulse generated in a titanium-doped sapphire, chirped pulse amplification laser system.[18] At best compression, the laser pulse had a 30–35 fs duration at full width at half maximum (FWHM). The pulse duration could be changed by translating one of the two gratings in the compressor. The laser energy was 1 J per pulse at central wavelength 820 nm. The beam was focused onto the edge of a 3 mm long supersonic helium gas jet using a f/18 off-axis parabola. The diffraction limited focal spot was $r_0=21$ μm at FWHM, producing vacuum-focused laser intensity of $I=3\times10^{18}$ W/cm^2, for which the corresponding normalized potential vector is $a_0=eA/(mc^2)=1.3$. For these high laser intensities, the helium gas was fully ionized by the foot of the laser pulse. At best compression, the laser pulse spatial dimensions were matched to the plasma wavelength: the pulse duration was 9–11 μm at FWHM and the transverse size was 21 μm at FWHM. We operated at a plasma density of $n_e=6\times10^{18}$ cm^{-3}, for which the plasma wavelength is $\lambda_p=13.6$ μm.

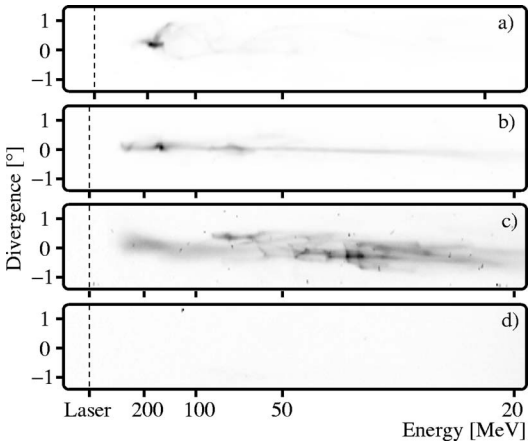

FIG. 1. Raw images of the electron beam obtained on the LANEX screen for a plasma density of $n_e=6\times10^{18}$ cm^{-3}. Panels (a) and (b) The pulse was at the best compression (duration 30–33 fs and intensity 3×10^{18} W/cm^2). (c) Pulse duration 40–45 fs, intensity $I=2-2.5\times10^{18}$ W/cm^2. (d) Pulse duration 60 fs, intensity $I=1.5\times10^{18}$ W/cm^2.

The electron beam properties were measured using an electron spectrometer consisting of a permanent magnet and a LANEX phosphor screen. The charge was monitored using a integrating current transformer. This setup has been described in previous publications.[12]

B. Experimental results

We present the electron beam distribution in energy and angle in Fig. 1 for different pulse durations. Figure 1 shows raw images that were obtained by imaging the LANEX screen. Panels (a) and (b) were obtained with the shortest laser pulses: the images show a very collimated electron beam with quasimonoenergetic features. In panel (c), the pulse was slightly chirped to 40–45 fs and this was enough to deteriorate the quality of the electron beam: the beam divergence is larger and the energy distribution is much broader, as the narrow peaks have disappeared. A likely interpretation of this is that a slightly longer pulse is enough to perturb the accelerated electrons and degrade the beam quality. However, for a 40–45 fs pulse, the intensity is decreased

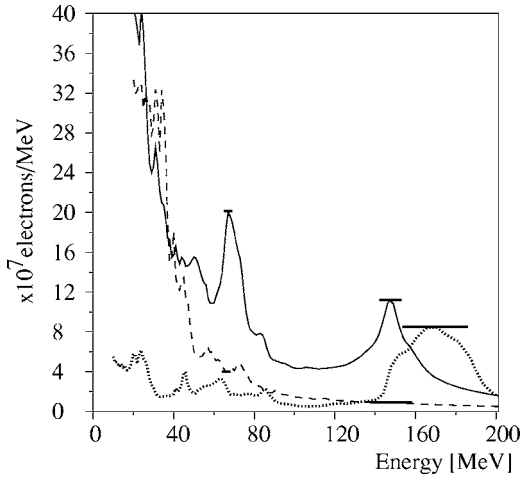

FIG. 2. Electron energy distribution obtained from the raw images of Fig. 1. The full curve and the dotted curve represent spectra for pulse durations of 30–33 fs; the dashed curve was obtained with a duration of 40–45 fs. The horizontal bars represent the spectrometer resolution for different electron energies.

from $I=3\times10^{18}$ W/cm^2 to $I=2-2.5\times10^{18}$ W/cm^2. This decrease in intensity might also have an effect on the interaction and on the quality of the electron beam. In the case of 50–60 fs pulses [see panel (d)], the intensity is too low and trapping of electrons does not occur. The electron beam energy distribution corresponding to the images of Fig. 1 are presented in Fig. 2. The full curve and the dotted curve were obtained for the same laser and plasma parameters: shortest pulse duration and highest intensity. Both spectra exhibit well-defined energy peaks but they are very different from each other. This is due to the fact that this regime of interaction is not stable yet: fluctuations in laser and plasma parameters (laser intensity and/or plasma density) still produce large fluctuations in the electron energy distribution.

These results clearly show that for our laser parameters, the best electron beam is obtained when the laser pulse is the shortest and when the intensity is the highest, as expected from the physics of the bubble regime. The crucial parameter is the ratio $c\tau/\lambda_p$. When this ratio is larger than 1, the quality of the electron beam is degraded. In a previous publication, we showed results obtained for a 30 fs laser pulse but with higher plasma densities.[16] In this case, the ratio was increased by decreasing λ_p. However, the observations were similar: when $c\tau/\lambda_p>1$, the electron beam quality is degraded.

III. LASER PULSE SHORTENING IN PLASMA WAVES

Another major phenomenon which occurs in the bubble regime is the self-compression of the laser pulse as it interacts with the plasma wave. This point is extremely important for two reasons: (i) the shortened laser pulse has a sharper front and excites a stronger wake field; (ii) the shortening of the laser pulse reduces the negative effect of the laser transverse electric field on the accelerated electrons. Self-compression was first seen in numerical simulations,[15,19–21] but it has never been observed directly in experiments. In Ref. 15, spectral broadening of the transmitted laser pulse was observed, and the authors indicated that this might have been a signature of laser pulse self-compression. However, further experimental evidence of this process was still necessary and a direct measurement will help remove ambiguities.

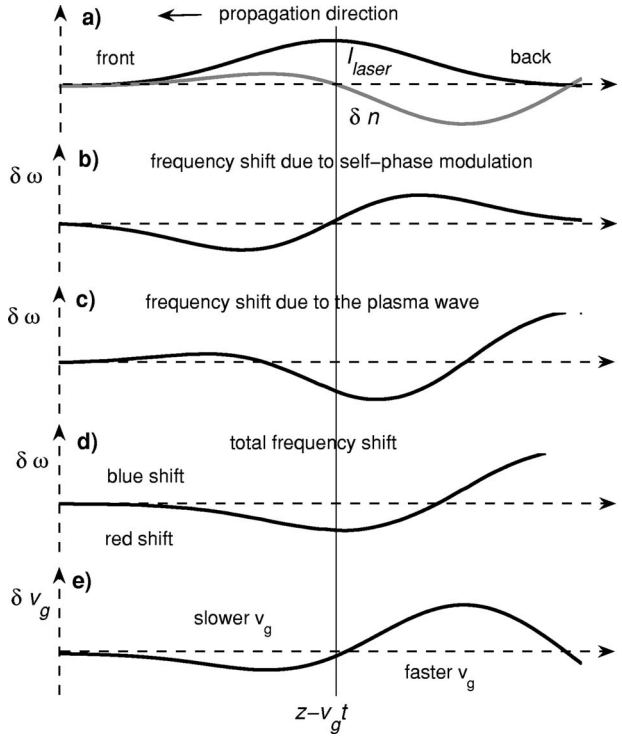

FIG. 3. Schematics illustrating spectral broadening and self-compression of a laser pulse in a plasma wave.

A. Physical mechanism

The physics of the self-compression mechanism can be understood by a simple 1D picture. In relativistic laser-plasma interactions, the index of refraction of the plasma can be written as $\eta(\xi)=1-(1+\delta n/n)\omega_p^2/\gamma\omega_0^2$, where $\xi=ct-z$, ω_p, and ω_0 are, respectively, the plasma and laser frequencies; $\delta n/n(\xi)$ is the normalized density perturbation due to the plasma wave. The term $\gamma\simeq(1+a^2/2)^{1/2}$ is the relativistic correction to the mass of electrons oscillating in the laser field, and a is the normalized vector potential. The term $1+\delta n/n$ is the correction to the index of refraction caused by the plasma wave. These corrections give rise to a collection of well-known effects for pulses longer than the plasma period (see Ref. 22 and references therein). For instance, the relativistic correction causes relativistic self-phase modulation (1D)[23] and relativistic self-focusing (2D).[24] Similarly, the plasma wave gives rise to Raman forward scattering (1D)[25] and the self-modulation instability (2D).[8–10]

Here, we are interested in the case where the pulse is shorter than the plasma wavelength ($c\tau<\lambda_p$). In this case, the above-mentioned instabilities are greatly reduced. The mechanism of pulse compression can be understood from the schematics of Fig. 3. An intense laser pulse drives a plasma wave [panel (a)]. The index of refraction of the plasma is modified by the laser through the relativistic factor γ. This

causes a frequency shift through relativistic self-phase modulation. This is illustrated in panel (b): the front of the pulse is redshifted, whereas the back is blueshifted. The plasma wave also modifies the index of refraction and as a consequence also causes frequency shifts; see panel (c). The sum of these two contributions is shown in panel (d): the front of the pulse is redshifted, whereas the back is blueshifted. Note that very short pulses fit completely into the first part of the plasma wave and, consequently, such pulses are mostly redshifted. Finally, the change in electron density due to the plasma wave also modifies the group velocity of the laser, as depicted in panel (e). As can be seen there, the front of the pulse tends to slow down, whereas the back catches up with the front, resulting in the compression of the laser pulse. As the pulse becomes compressed, it becomes essentially redshifted because it stays in the descending slope of the plasma wave.[20] Note that this physics is analogous to the soliton effect taking place in optical fibers.

In reality, a 1D description of this problem is not sufficient because 2D effects such as self-focusing can be important and the geometry of the excited wake fields is essentially three-dimensional. In fact, recent particle-in-cell (PIC) simulations have shown that, for large focal spots ($r_0 > \lambda_p$, where r_0 is the laser radius at FWHM), Raman side scatter tends to disrupt the laser pulse and causes transverse filamentation.[19,26] In order to avoid this effect, the laser waist should also be matched to the plasma wavelength.

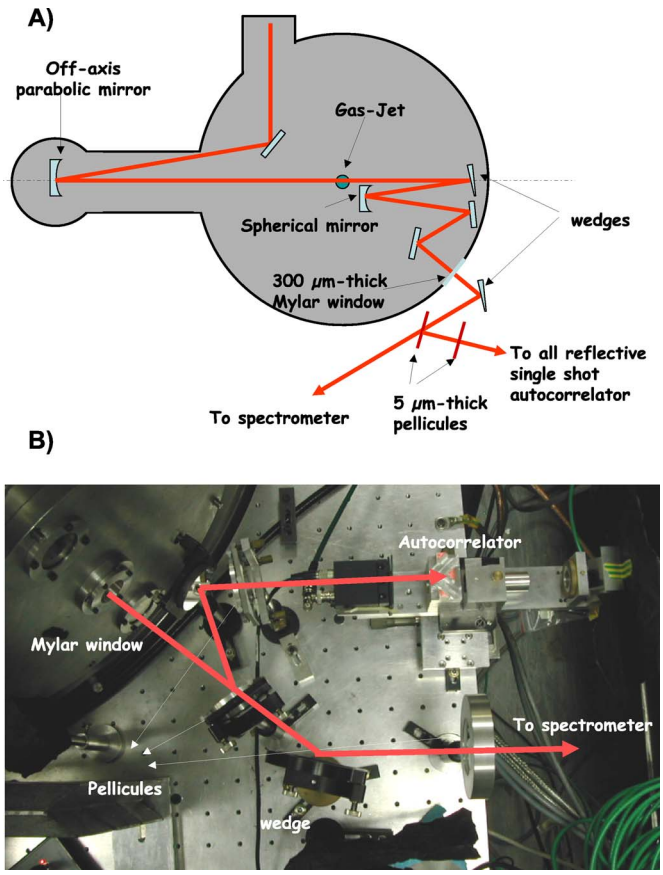

FIG. 4. (a) Schematics of the experimental setup which was used for the measurement of laser pulse shortening. (b) Picture of the compact single shot autocorrelator.

B. Experimental results

The measurement of pulse shortening was carried out for laser and plasma parameters very similar to the ones of Sec. II. However, in this particular experimental campaign, the laser pulse was slightly longer: $\tau = 38 \pm 2$ fs. The best shortening of the laser pulse with the best reproducibility was observed for $n_e = 6-7.5 \times 10^{18}$ cm^{-3}, for which the plasma wavelength ($\lambda_p = 12.2-13.6$ μm) is comparable with the laser pulse length ($c\tau = 11$ μm). The diameter was larger than the plasma wavelength, but one may expect that self-focusing in the plasma brings it down to the matched value, so that filamentation was not a critical issue.

In order to evaluate the effect of laser pulse shortening, the transmitted laser spectrum and the pulse autocorrelation were measured simultaneously on every shot. We found two experimental indications that the laser pulse was shortened in the plasma: (i) through measurements of the pulse spectral broadening; (ii) through direct measurement of the pulse duration using a single-shot intensity autocorrelator. The transmitted light spectrum was measured using an imaging visible spectrometer. The details of the experimental setup are shown in Fig. 4(a). More details can be found in Ref. 27. The autocorrelator consisted of a 50 μm thick type-I BBO crystal. The beam was separated into two parts by a reflective prism; each half-beam was sent on the BBO crystal with a 5° incidence angle. This gave a geometrical resolution of 2 fs, but phase matching in the 50 μm thick BBO crystal limited the spectral bandwidth which can be frequency doubled and thus limited the minimum measurable duration to 10 fs. A picture of the compact autocorrelator that we used is shown in Fig. 4(b).

Figure 5 shows the transmitted spectra for different plasma densities. The bottom curve shows the initial laser spectrum: its width at FWHM is 35 nm. As long as the ratio $c\tau/\lambda_p$ stays close to 1, the interaction is close to resonance and the laser spectrum is considerably broadened because of the frequency shifts caused by the plasma wave and by relativistic self-phase modulation (this can be seen in Fig. 5 for $n_e < 10^{19}$ cm^{-3}). The strong redshift is significant of the excitation of a high amplitude plasma wave. The laser spectrum is broadened to 100–150 nm at FWHM, depending on plasma density, and it extends over 250 nm. Therefore, for such spectra, the transform limited pulse length at FWHM could be as short as 7–8 fs. As the density is increased, the broadening becomes less important because the redshift is smaller. At high plasma density, the laser spectrum is blueshifted by about 20 nm (see the spectrum at $n_e = 4 \times 10^{19}$ cm^{-3}).

However, even though spectral broadening is consistent with shorter pulses, it does not prove that the pulses are shorter. Hence, direct measurements of the pulse duration are necessary. In Fig. 6 we present the autocorrelation measurements. Figure 6(a) shows lineouts of the autocorrelation traces. Here, the pulse is clearly shortened after interacting with the plasma: the vacuum autocorrelation FWHM is

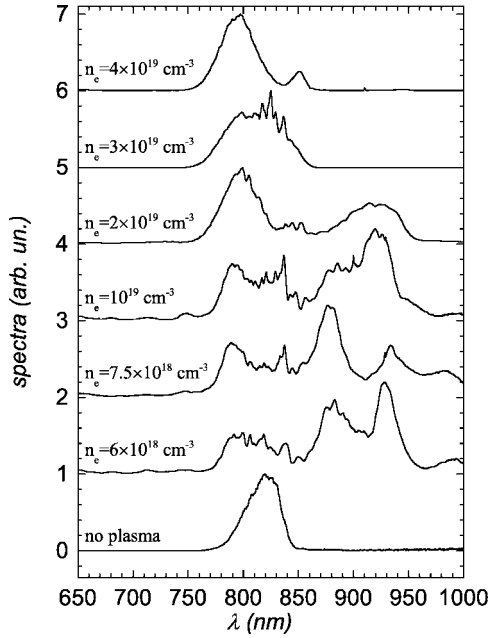

FIG. 5. Transmitted laser spectra for different plasma densities.

53±2 fs (assuming a Gaussian pulse shape, this gives a FWHM of 38±2 for the incident laser pulse). When the pulse interacts with the plasma at density 7.5×10^{18} cm^{-3}, the FWHM of the autocorrelation is shortened to 14±2 fs.

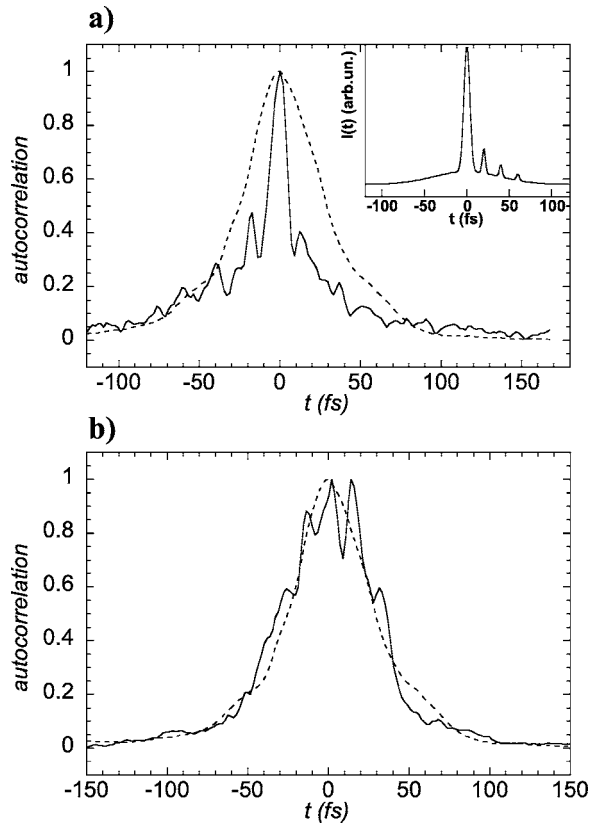

FIG. 6. (a) Lineouts of autocorrelation traces. Dashed line: autocorrelation for a zero plasma density, full line: autocorrelation for $n_e=7.5\times10^{18}$ cm^{-3}. The inset represents a possible pulse shape. (b) Same as (a) but the full line was obtained for $n_e=10^{19}$ cm^{-3}.

The exact pulse duration cannot be known because one has to assume a pulse shape in order to compute the pulse duration. A Gaussian pulse would give a FWHM of 9.9±1.4 fs (close to the autocorrelator resolution), whereas a square pulse would give a FWHM of 14 fs. Thus, one can conclude that the duration after interaction with the plasma is (10 −14)±2 fs FWHM. Here, the longest duration (14 fs) corresponds to the worst case scenario (a square pulse) and the shortest (10 fs) to the best case scenario (a Gaussian pulse, and also the autocorrelator resolution limit). Figure 6(b) shows similar curves for a plasma density of 10^{19} cm^{-3}. In this case, the laser pulse was not shortened but merely modulated. Similar results are obtained when the pulse duration is increased: we have never observed pulse shortening for pulse lengths longer than the plasma wavelength.

The inset of Fig. 6(a) presents a possible pulse shape which has been optimized to fit the measured autocorrelation. Mathematically, it is impossible to compute the pulse shape from its autocorrelation: this problem does not have a unique solution. However, the presence of peaks in the autocorrelation suggests peaks in the intensity temporal profile. For instance, one can obtain a main pulse followed by three peaks. This effect can be explained by the fact that the laser pulse is slightly too long to completely fit in a single plasma period: the pulse length is 38 fs at FWHM but about 70 fs at $1/e^2$. This could cause a residual self-modulation of the pulse. One could also imagine a pulse shape with a peak before the main pulse. Such a front peak in the intensity profile could be due to defocusing of the very front of the pulse by the plasma wave. In this case, the front of the pulse would be diffracted away but it would still appear as a side peak in the autocorrelation. The side peaks could also be due to the presence of high order phase terms which prevent a perfect compression. For instance, a large and uncompensated third-order phase term results in side modulations of the laser envelope.

Another important point to consider is the overall energy efficiency of this mechanism. Using near-field imaging of the laser beam and far-field imaging on the spectrometer, we estimated that 30–50% of laser energy was dumped into the plasma, 10–30% was scattered outside of the collection angle (f/18), and 40%±10% was transmitted through the plasma, collected, and sent to the autocorrelator. Assuming that the pulse temporal profile is given by the inset in Fig. 6(a) and that it stays similar across the spatial distribution of the laser beam, then the main peak contains about 50% of the transmitted laser energy. Under these assumptions, the energy in the main peak is found to be 200±50 mJ, which represents an overall compression efficiency of 20±5%.

These results show that pulse shortening from 38±2 fs down to 10−14±2 fs is possible when the laser pulse is close to resonance with the plasma wave (e.g., $c\tau/\lambda_p\simeq1$). Laser pulse shortening occurs for parameters where the quality of the electron beam is the highest, as predicted in simulations of the bubble regime.[17]

IV. EVIDENCE OF ULTRASHORT STRUCTURES IN THE ELECTRON BUNCH

As mentioned earlier, the production of ultrashort electron bunches is of particular interest for a large range of applications where time resolution is required. In principle, relativistic laser-plasma interaction in the regime we have described throughout this paper is able to produce such sub-100 fs bunches. Simulations have indicated that bunches as short as 10–30 fs can be produced in the bubble regime.[12,13] However, measuring these bunches in the laboratory is a real challenge. Previous work has shown that electro-optic sampling[28,29] of the electron bunch electric field can give a direct measurement of the bunch duration.[30,31] In this case, the electric field of the electron bunch induces birefringence in a nonlinear crystal placed close to the beam. This induced birefringence can be inferred by measuring the polarization of a probe laser beam going through the nonlinear crystal. However, because of practical limitations linked to the geometry of this method, the resolution of this technique can hardly reach 100 fs, which is not sufficient for our case. Another technique relies on the transition radiation[32] of the electron bunch.

Transition radiation (TR) is the radiation which is emitted by a particle going through an interface. The radiation is said to be incoherent when the bunch size is longer than the emitted wavelength: electrons generate transition radiation at random phases and the radiated fields do not add up coherently. In this case, the radiation emitted by the beam is simply the sum of the radiation emitted by each individual electron. On the other hand, when the bunch size is shorter than the wavelength of emission, electrons radiate in phase and the radiation adds up coherently. In consequence, the coherent signal scales as N^2 (where N is the number of particles in the bunch) and it is orders of magnitude larger than the incoherent signal. Roughly speaking, the spectrum of the coherent transition radiation (CTR) is then the Fourier transform of the bunch shape. Thus, measuring the spectrum gives information on the bunch shape and consequently on the bunch duration. For instance, by measuring coherent transition radiation at $\lambda = 10\ \mu$m, one can infer that the electron bunch has 30–50 fs structures in its temporal profile. In reality, in order to retrieve exact information from the transition radiation spectrum, one has to use a full model where many parameters can play a role. The theory of coherent transition radiation emitted by an arbitrary electron beam is given in the Appendix.

Transition radiation depends on many different factors and it is only useful as a diagnostic if all of the crucial parameters are measured precisely. The following quantities should be known in order to model the problem properly: (i) the geometry of the problem: collection angles, size of the radiator, type of radiator; (ii) the electron beam transverse distribution; (iii) the energy distribution of the electron beam. If these quantities are measured, then the only unknown of the problem is the electron bunch temporal shape. Thus, by fitting the model to the experimental results, one can retrieve information on the bunch shape. For these experiments, the spectrum of the emitted radiation can be measured directly with a spectrometer[33,34] or by Fourier transform interferometry.[36] Note that the transition radiation spectral content can also be measured in the time domain by electro-optic sampling.[35] However, the time resolution of this method is limited by the laser probe pulse duration (typically 30–50 fs for the laser systems that are used in these experiments) or by phase mismatch in the nonlinear crystal (10–1000 fs depending on crystal thickness).

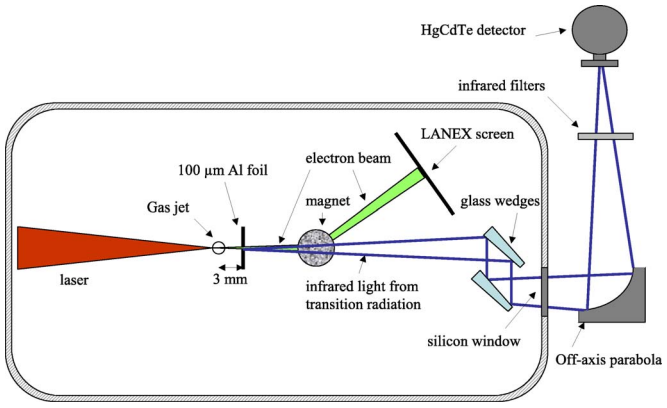

FIG. 7. Experimental setup.

In accelerator and beam physics, the measurement of coherent transition radiation is a well-known method for characterizing short electron bunches.[36,37] More recently, it has also been used in laser-solid target experiments in order to diagnose microstructures of the laser accelerated electrons.[33,38] In the context of laser-plasma accelerators, coherent transition radiation has been used for generating a bright THz source in the far-infrared region (100 μm).[34,39] In Ref. 39, the authors briefly mentioned that their measurement of coherent radiation was consistent with sub-100 fs electron bunches. However, these measurements were essentially done in the 0.1–1 mm range, where little information can be obtained about very short bunch structures: 10–100 fs structures correspond to 3–30 μm wavelengths.

In what follows, we present spectral measurements of coherent transition radiation in the 8–10 μm range. The results suggest sub-50 fs structures in the electron bunch. Note that these measurements were performed using a highly collimated and high energy electron beam, unlike Ref. 39, where the electron beam had a Maxwellian energy distribution.

A. Experimental results

The experimental setup is described schematically in Fig. 7. The electron beam is generated during the interaction of the laser with the gas jet. A 100 μm thick aluminum foil was placed 3 mm behind the gas jet. The foil acted as a radiator for transition radiation when the electron beam passed through it. It also blocked the laser light and prevented it from propagating to the detectors.

The electron beam angular and energy distribution were measured on each shot with the electron spectrometer described earlier. The electron beam divergence was obtained by turning off the magnet on the spectrometer. The beam had

a near-cylindrical symmetry and had a typical divergence of 8 ± 1.5 mrad FWHM. The electron spectrum shows quasimonoenergetic spikes and electron energies extending up to about 200 MeV. The position of the spikes varied from shot to shot but the overall charge in the 20–200 MeV range stayed close to about 1 nC. Note that, knowing the angular distribution of the beam and assuming a ballistic propagation, one can compute its transverse distribution at the radiator location.

Transition radiation of the electron beam passing through the foil produced infrared radiation (IR) which was detected using a nitrogen-cooled HgCdTe infrared detector. The detector is sensitive to wavelengths shorter than 12 μm. Above 12 μm, the sensitivity of the detector drops dramatically. The detector was calibrated using a Ti:sapphire laser at 800 nm. This provided an absolute calibration at all wavelengths because the detector spectral response was given by the manufacturer.

The IR light was collected and focused onto the detector using an off-axis parabola. The collection angle was $\theta_0 = 10$ mrad. Note that this narrow collection angle has consequences for the interpretation of the data. First, most of the radiation emitted along this narrow solid angle comes from electrons with energies >50 MeV [see Eq. (A2) in the Appendix]. Thus, in this configuration, we are only considering the "interesting" electrons (the high energy ones). Note also that in this particular case, the shape of the electron spectrum does not influence greatly the amount of radiated signal: only the number of high energy electrons is important. Second, one can show that with such a geometry, the transverse distribution of the electron beam does not play a big role in the production of coherent transition radiation [see Eq. (A9) in the Appendix]. Indeed, the transverse distribution of the beam does not have to be measured as long as the transverse size σ_r is such that $\sigma_r \ll \lambda / \pi\theta_0$, where λ is the wavelength of the radiation. This condition is always true in our experiment and the transverse extent of the electron beam has no consequence on the magnitude of the coherent transition radiation signal.

Various filters were added to the beam path in order to cut all laser light: a germanium filter insured that the light below 1.6 μm was attenuated by more than 10^4. Similarly, the IR radiation was coupled out of the vacuum chamber using a 3 mm thick, high resistivity silicon window. Two glass wedges were used to reflect the IR light and to damp visible laser light. Typically, glass reflects strongly at 7–10 μm wavelengths. All filters (including glass wedges, germanium and silicon windows) were carefully calibrated using various infrared spectrophotometers: first in the range 0.5–3 μm and then in the range 2.5–50 μm). An interferential IR filter was added in order to select a specific spectral bandwidth. The transmission of this IR filter is shown in Fig. 8(a), whereas the transmission of the whole optical system is shown in Fig. 8(b). Wavelengths below 3 μm are attenuated by more than 10^{-12}. The transmission is highest for wavelengths in the 8–10 μm. This is mostly due to absorption in the glass wedges and the interferential IR filter.

A strong optical signal at 8–10 μm was detected when the interaction produced a high energy electron beam.

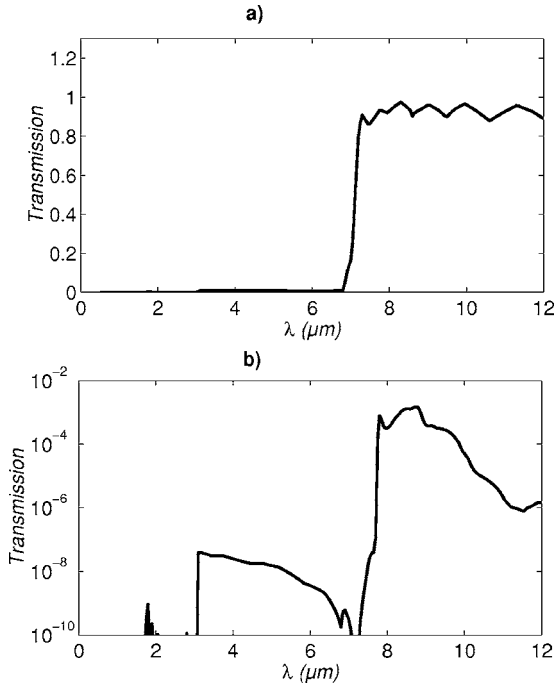

FIG. 8. (a) Transmission of the infrared interferential filter which was used in order to isolate the wavelength range of interest. (b) Transmission of the whole optical system, including reflections on glass wedges, transmission through several silicon filters, germanium filters, and the interferential filter.

Simple null tests were performed in order to insure that the signal from the IR detector was really due to photons at 8–10 μm: (i) no signal was observed when the beam path was blocked; (ii) no signal was observed when the gas jet was turned off (in this case, the defocused laser beam interacted directly with the aluminum foil); (iii) adding a $T = 30\%$ silicon filter caused a signal reduction of a factor of 3, as expected for IR light around 10 μm. Figure 9 shows the correlation between the transition radiation signal and the number of high energy electrons when various parameters of the interaction were changed. The electron beam can be optimized for highest electron energy and highest spatial quality by adjusting the gas jet position, the laser pulse duration, and the electron plasma density. The black diamonds in Fig. 9(a) represent the number of electrons above 50 MeV as a function of plasma density. As expected, the signal is the largest when the plasma density is $n_e \simeq 5 \times 10^{18}$ cm^{-3}, for which the ratio $\tau c / \lambda_p = 0.7 < 1$. The empty circles represent the IR signal level, which is very well correlated to the high energy electron signal. This is because, as we have seen earlier, the level of transition radiation in the 10 mrad collection angle depends critically on the number of high energy electrons in the beam. The noise level for the IR signal was very high (about 30% of the signal itself). This was due to the presence of a strong radio-frequency (rf) noise occurring during the interaction. This noise was also fluctuating from shot to shot and it tended to decrease the dynamic range of the detection. In Fig. 9, we have represented the impact of this noise on the IR signal by the left error bars on the empty circles. The middle error bars correspond to statistical fluctuations.

Figure 9(b) shows a similar correlation between the

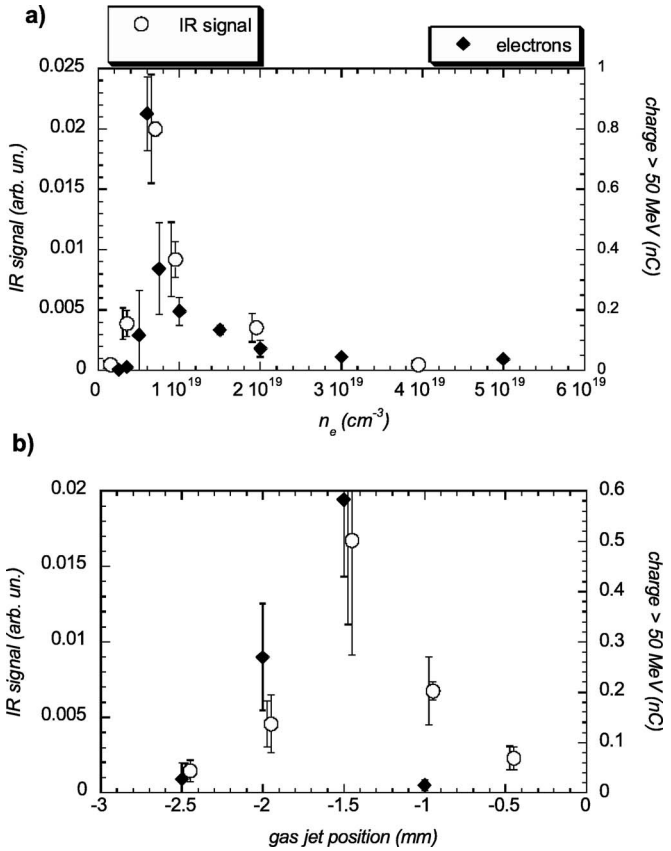

FIG. 9. Dependence of infrared signal with experimental parameters. The empty circles represent the signal detected with the HgCdTe detector; the full diamonds represent the charge for electrons with energies greater than 50 MeV. Each dot is an average of 3–5 shots. The empty circles have two error bars: the left ones come from the rf noise; the middle ones come from statistical fluctuations. (a) Variation of IR signal when the plasma density is changed. (b) Variation of IR signal when the gas jet position with respect to the laser focus is varied.

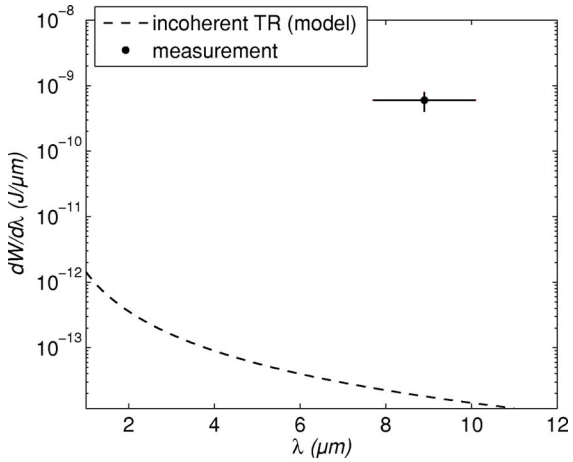

FIG. 10. Comparison between the signal level modeled using incoherent transition radiation (dashed line) and the measurement (full circle). The horizontal error bar indicates the wavelength range of the detection. The vertical error bar represents shot to shot fluctuations over 5 shots.

amount of high energy electrons and IR signal when the position of the gas jet is moved. The highest signal is obtained for the position −1.5 mm, for which the laser pulse is focused at the edge of the nozzle. This optimized gas jet position insures optimal coupling between the laser and the gas jet, and produces a high quality electron beam as well. In all cases, the highest transition radiation signal is obtained for the best electron beam (small divergence angle, high charge at high energy).

In principle, the coherent nature of the radiation can be determined by varying the charge Q of the electron beam. If the amount of radiation scales as Q^2, then it is coherent. However, in the present experiment, it was impossible to vary the charge without changing other parameters. For instance, in Fig. 9 the charge is varied by changing the plasma density, but the energy distribution, the divergence, and possibly the bunch duration also change. In these conditions, there is no reason to expect a quadratic dependence of the IR signal with the charge. In addition, the large error bars that we obtained on the charge and the IR signal do not give us enough precision for trying to determine such trends. In the present experiment, we determined the coherent nature of the radiation through the number of photons emitted in the transition radiation process.

Taking into account the transmission of the filters as well as the calibration of the detector, one can compute that the energy produced by transition radiation was $dW/d\lambda \simeq (6.5\pm2)\times10^{-10}$ J/μm in the 8–10 μm range. Figure 10 shows the detected energy level versus modeling of incoherent transition radiation, using Eq. (A4) of the Appendix. The measured signal is more than three orders of magnitude higher, proving that it is at least partially coherent. In the next section, we will see how this coherent transition radiation signal allows us to retrieve temporal information regarding the electron bunch.

B. Discussion of the results

The fact that the transition radiation (TR) signal is coherent or partially coherent in the 8–10 μm range implies that the electron bunch has temporal structures in the 30 fs range. We used Eq. (A6) in order to fit the measured signal. Since the temporal distribution of the bunch is unknown, one has to assume a bunch temporal profile in order to obtain an idea of the bunch duration. In fact, there is an infinite number of possibilities and pulse shapes that can fit the data. In the following, we have used realistic pulse shapes, such as Gaussian, super-Gaussian, Lorentzian, and sech.[2] We have also considered the possibility of two bunches separated by the plasma wavelength $\lambda_p = 13.6$ μm. This case is of particular interest because simulations have indicated that, depending on the plasma density, several bunches can be accelerated in the first arches of the plasma wave. This means that the bunch can be composed of a few microbunches separated by the plasma wavelength. We have looked at two characteristic time scales: the FWHM of the electron bunch, and the rise time, defined as the time it takes to go from 20% to 80% of the maximum electron density. The results are shown in Table I. In all cases, the rise time is shorter than 40 fs, whereas the bunch FWHM is shorter than 100 fs. The short-

TABLE I. Table showing the dependence of electron bunch rise time and duration at FWHM for different pulse shapes. "Double Gaussian" refers to two Gaussian electron bunches separated by λ_p=13.6 μm.

Shape	Rise time (fs)	FWHM (fs)
Gaussian	18	37
Lorentzian	42	55
Super-Gaussian	20	81
Sech^2	24	44
Double Gaussian	16.5	78
Double Lorentzian	32	86
Double sech^2	19	79

est bunch duration is obtained for a Gaussian pulse: 18 fs rise time and 37 fs FWHM, whereas the worse case is for the super-Gaussian shape: 20 fs rise time and 81 fs FWHM.

Figure 11(a) shows two possible pulse shapes which could explain the coherent transition radiation (CTR) signal observed around 10 μm. The Gaussian shape and the Lorentzian shape can both fit the measured signal. Figure 11(b) shows the slightly different IR spectra that these different bunch shapes generate. As can be seen in the figure, the radiation begins to become coherent for wavelengths greater than 6(4) μm for a Gaussian (Lorentzian) shape. Finally, Fig. 11(c) and Fig. 11(d) show that a double-humped electron bunch can also fit the measured signal.

From these data, it is impossible to determine precisely which bunch shape corresponds best to the experiment because the measurement was done in a narrow spectral range. Measuring the whole infrared spectrum might give more information on the bunch shape. Future work will focus on measuring transition radiation in a broader range of wavelengths.

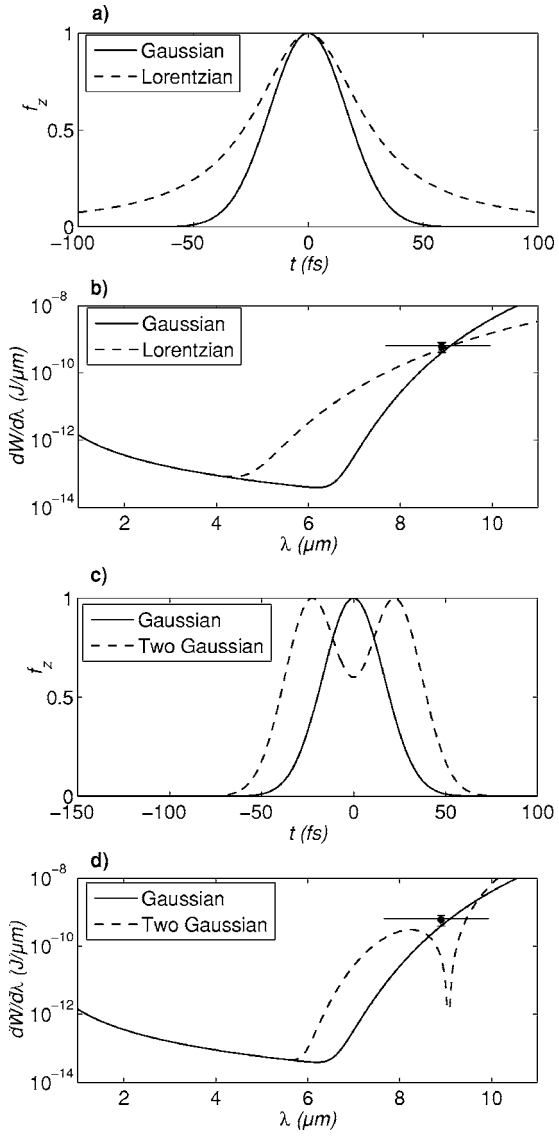

FIG. 11. (a) Two possible shapes for the electron bunch: a Gaussian bunch (full line) and a Lorentzian bunch (dashed line). Both shapes reproduce the measured signal when the coherent transition radiation spectrum is calculated. (b) Comparison between the measured IR signal and coherent transition radiation models for different electron bunch shapes. (c) Same as above with a Gaussian bunch (full line) and two Gaussian bunches separated by λ_p (dashed line). (d) The transition radiation spectrum emitted for the Gaussian (full) and double Gaussian pulse (dashed).

V. CONCLUSION

In conclusion, we have studied experimentally the interaction of an ultrashort laser pulse with an underdense plasma in the relativistic regime. This interaction produces a high quality, high energy electron beam when the shortest and highest intensity laser pulses are used (1 J of energy, with a duration of 30 fs). We have seen that the best electron beams are produced in the so-called bubble regime, where the spatial dimensions of the beam are comparable to or smaller than the plasma wavelength. When this condition is realized, other nonlinear ultrafast phenomena occur: the laser pulse spectral broadening and redshifting, as well as its temporal shortening from 38 fs down to 10–14 fs. Finally, we have investigated the temporal aspect of the electron bunches produced by these short laser pulses. The measurement of the coherent transition radiation of the electron beam going through a metallic foil has given evidence of sub-50 fs temporal structures in the electron bunch. This work is the result of the continuing effort to develop, optimize, and diagnose the new electron sources that can be obtained in laser-plasma accelerators.

ACKNOWLEDGMENTS

J.F. thanks P. Audebert and J.-P. Geindre for discussions and help with the autocorrelator.

The authors acknowledge the support of the LOA laser team as well as the support of the European Community Research Infrastructure Activity under the FP6 "Structuring the European Research Area" Program (CARE, Contract Number RII3-CT-2003-506395).

APPENDIX: A MODEL FOR THE TRANSITION RADIATION PRODUCED BY ARBITRARY ELECTRON BEAMS

The goal of this section is to model the radiation produced by an electron bunch going through a metal foil.[32] The

radiator (the metal foil) is assumed to be a conductor of infinite size. The electron beam has cylindrical symmetry, as was measured in the experiment. The model described here was largely inspired by previously published work.[40,41]

1. Radiation of a single electron

Let us first consider the radiation of a single electron. The geometry of the problem is illustrated in Fig. 12: an electron exits the radiator at an angle ψ, with azimuthal angle ϕ. The radiation emitted in the solid angle $d\Omega$ at angle θ is given by

$$\frac{d^2W}{d\omega d\Omega} = \frac{e^2}{\pi^2 c}(\varepsilon_\parallel^2 + \varepsilon_\perp^2), \tag{A1}$$

where e is the charge of the electron, c the velocity of light, and $\varepsilon_\parallel$ and $\varepsilon_\perp$ are functions of the electron velocity $\beta = v/c$ as well as angles ψ, ϕ, and θ. $\varepsilon_\parallel$ and $\varepsilon_\perp$ are the normalized transition radiation fields defined as follows:

$$\varepsilon_\parallel = \frac{\beta_z \cos\theta |1-\epsilon|}{[(1-\beta_x \cos\theta_x)^2 - \beta_z^2 \cos^2\theta]\sin\theta} \times \left| \frac{(1-\beta_z\sqrt{\epsilon - \sin^2\theta} - \beta_z^2 - \beta_x \cos\theta_x)\sin^2\theta + \beta_x\beta_z \cos\theta_x \sqrt{\epsilon - \sin^2\theta}}{(1-\beta_x\cos\theta_x - \beta\sqrt{\epsilon - \sin^2\theta})(\sqrt{\epsilon - \sin^2\theta} + \epsilon\cos\theta)} \right|,$$

$$\varepsilon_\perp = \frac{\beta_x \beta_z^2 \cos\theta_y \cos\theta |1-\epsilon|}{[(1-\beta_x \cos\theta_x)^2 - \beta_z^2 \cos^2\theta]\sin\theta} \times \left| \frac{1}{(1-\beta_x\cos\theta_x - \beta_z\sqrt{\epsilon - \sin^2\theta})(\sqrt{\epsilon - \sin^2\theta} + \cos\theta)} \right|,$$

with

$$\beta_x = \beta \sin\psi,$$

$$\beta_z = \beta \cos\psi,$$

$$\cos\theta_x = \sin\theta\cos\varphi,$$

and

$$\cos\theta_y = \sin\theta\sin\varphi.$$

In the case of a relativistic electron exiting a perfect conductor at normal incidence, Eq. (A1) reduces to the well-known expression

$$\frac{d^2W}{d\omega d\Omega} = \frac{e^2}{\pi^2 c}\frac{\beta^2 \sin^2\theta}{(1-\beta^2\cos^2\theta)^2}. \tag{A2}$$

From this equation, it follows that transition radiation is emitted along a cone with half-angle $\theta \simeq 1/\gamma$, where γ is the relativistic factor of the electron. For example, 50 MeV electrons emit radiation within a cone of 10 mrad half-angle.

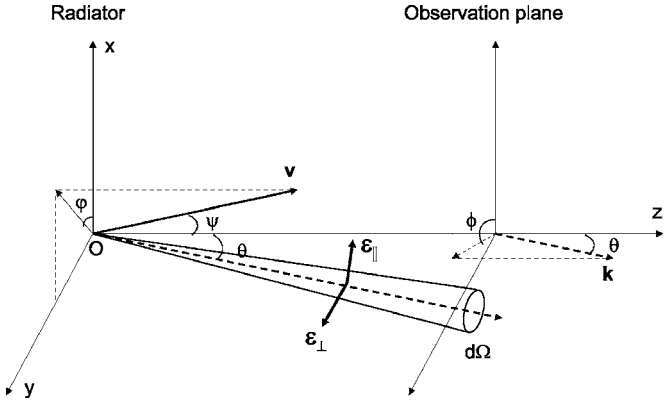

FIG. 12. Geometry of the radiation emitted by an electron when exiting the radiator. The electron exits the radiator along vector **v**, at angle ψ and azimuthal angle ϕ. The radiation is collected in solid angle $d\Omega$ along vector **k**, at angle θ with the radiator plane.

2. Radiation produced by an electron beam

The electron bunch can be represented by its six-dimensional distribution function $h(\mathbf{x},\mathbf{p})$, where **x** and **p** are, respectively, the position and momentum of a particle. We now assume that there is no correlation between the position of an electron in the bunch and its momentum. Thus, the bunch can be represented by a spatial distribution $f(\mathbf{x})$ and a momentum distribution $g(\mathbf{p})$, such that $h(\mathbf{x},\mathbf{p}) = f(\mathbf{x}) \times g(\mathbf{p})$.

We also assume that there is no correlation between the transverse and longitudinal position of electrons in the bunch, so that the spatial distribution function can be represented by a transverse distribution $f_r(\mathbf{r})$ and a longitudinal distribution $f_z(z)$, with $f(\mathbf{x}) = f_r(r) \times f_z(z)$.

Similarly, we assume that there is no correlation between the energy of an electron and its angle. In this case, the momentum distribution function can be written as $g(\mathbf{p}) = g_\psi(\psi) \times g_\phi(\phi) \times g_u(u)$, where $u = \|\mathbf{p}\|/mc$ is the normalized electron momentum.

In the context of electron beams generated in laser-plasma accelerators, these assumptions are reasonable as long as the electron beam generates transition radiation before it has propagated too long. After propagation over a long distance, the most energetic electrons tend to be at the front of the bunch and around the propagation axis, whereas the less energetic electrons are at the back and off to the sides. However, our experimental electron beam is very collimated

and electrons have very high energies, so that at the radiator location these assumptions of uncorrelated distribution functions are very reasonable.

The radiation is said to be incoherent when the bunch size is longer than the emitted wavelength: electrons generate transition radiation at random phases and the radiated fields do not add up coherently. In this case, the radiation emitted by the beam is simply the sum of the radiation emitted by each individual electron, over the distribution function. This reads

$$\left.\frac{d^2W}{d\omega d\Omega}\right|_{\mathrm{INC}} = \frac{e^2N}{\pi^2c} \times \int d^3\mathbf{p}(\varepsilon_\parallel^2 + \varepsilon_\perp^2)g(\mathbf{p}), \tag{A3}$$

where N is the number of electrons in the bunch. This equation can be written more explicitly as

$$\left.\frac{d^2W}{d\omega d\Omega}\right|_{\mathrm{INC}} = \frac{e^2N}{\pi^2c}\int_0^{+\infty} du g_u(u)\int_0^{2\pi} d\varphi g_\varphi(\varphi) \times \int_0^{\pi/2} d\psi g_\psi(\psi)(\varepsilon_\parallel^2 + \varepsilon_\perp^2). \tag{A4}$$

When the bunch size is comparable to the wavelength of emission, the electrons radiate in phase and the radiation adds up coherently. In consequence, the coherent signal scales as N^2 and it is orders of magnitude larger than the incoherent signal,

$$\left.\frac{d^2W}{d\omega d\Omega}\right|_{\mathrm{COH}} = \frac{e^2N(N-1)}{\pi^2c} \times \left[\left|\int d^3\mathbf{p}\varepsilon_\parallel g(\mathbf{p})F\right|^2 + \left|\int d^3\mathbf{p}\varepsilon_\perp g(\mathbf{p})F\right|^2\right]. \tag{A5}$$

Here, F stands for the form factor which defines the level of coherence of the emitted signal. For example, when the electron bunch is much smaller than the emitted wavelength, the radiation is fully coherent and $F=1$. In the case of uncorrelated distribution functions, one defines the transverse and longitudinal form factor F_r and F_z, with $F=F_r\times F_z$. The form factors are defined as

$$F_r(\omega,\theta) = \int d^2\mathbf{r}e^{-i\mathbf{k_r}\cdot\mathbf{r}}f_r(\mathbf{r}),$$

$$F_z(\omega,\theta,\phi,\psi) = \int dz e^{-i(\omega-\mathbf{k_r}\cdot\mathbf{v_r})z/v_z}f_z(z).$$

For an electron bunch with cylindrical symmetry, the integral over $\varepsilon_\perp$ cancels out and Eq. (A5) can be simplified to

$$\left.\frac{d^2W}{d\omega d\Omega}\right|_{\mathrm{COH}} = \frac{e^2N(N-1)}{\pi^2c}\left|\int_0^{+\infty} du g_u(u)F_r\int_0^{\pi/2} d\psi g_\psi \times \int_0^{2\pi} d\varphi g_\varphi\varepsilon_\parallel F_z\right|^2. \tag{A6}$$

In the experiment, all the distribution functions are measured (g_u: electron energy distribution, g_ψ and g_ϕ: electron beam divergence, f_r: transverse spatial distribution). The only distribution which is not measured is the longitudinal distribution f_z, which contains all the information on the bunch temporal shape and duration. Thus, by measuring parts of the spectrum where the transition radiation is coherent, one can obtain information on the distribution function f_z. For instance, by measuring coherent transition radiation at $\lambda=10$ μm, one can infer that the electron bunch has 30 fs structures in its temporal profile. By matching the model with the experiment, one can obtain more detailed information and one can retrieve possible temporal shapes for the electron bunch. However, this method does not provide an accurate measurement of the bunch duration; it only gives a range of possible bunch shape and durations.

The final quantity which will be compared to experimental results is the transition radiation spectrum emitted into a collection angle defined by the half-angle θ_0,

$$\frac{dW}{d\omega} = 2\pi\int_0^{\theta_0} \sin\theta d\theta\left(\left.\frac{d^2W}{d\omega d\Omega}\right|_{\mathrm{INC}} + \left.\frac{d^2W}{d\omega d\Omega}\right|_{\mathrm{COH}}\right). \tag{A7}$$

For practical purposes, the bunch divergence will be modeled by the following distributions:

$$g_\phi = \frac{1}{2\pi},$$

$$g_\psi = A\cos\psi e^{-\psi^2/\sigma_\psi^2},$$

where A is a normalization constant and σ_ψ is the radius of the angular distribution. The electron energy distribution g_u is taken from the measured distribution function. Finally, the transverse spatial distribution is modeled as follows:

$$f_r = \frac{1}{2\pi\sigma_r^2}\exp[-r^2/(2\sigma_r^2)], \tag{A8}$$

which gives the following form factor:

$$F_r(\lambda,\theta) = \exp[-2\pi^2\sigma_r^2\sin^2\theta/\lambda^2]. \tag{A9}$$

Note that for our experimental parameters, the collection half-angle is very small: $\theta_0=10$ mrad. In this case, the transverse form factor can be set to $F_r=1$ as long as $\sigma_r \ll \lambda/\pi\theta_0$. This condition is always true in our experiment, and in consequence the transverse extent of the electron beam has no consequence on the magnitude of the coherent transition radiation signal. Hence, the bunch duration is the only responsible factor for decreasing the level of coherent transition radiation.

[1] A. Modena, A. Dangor, Z. Najmudin, C. Clayton, K. Marsh, C. Joshi, V. Malka, C. Darrow, D. Neely, and F. Walsh, Nature (London) **377**, 606 (1995).
[2] D. Umstadter, S.-Y. Chen, A. Maksimchuk, G. Mourou, and R. Wagner, Science **273**, 472 (1996).
[3] Y. Gauduel and P. Rossky, *Ultrafast Reaction Dynamics and Solvent Effects* (AIP, New York, 1994).
[4] B. Brozek-Pluska, D. Gliger, A. Hallou, V. Malka, and Y. A. Gauduel, Radiat. Phys. Chem. **72**, 149 (2005).
[5] J. Belloni, H. Monard, F. Gobert *et al.*, Nucl. Instrum. Methods Phys. Res. A **539**, 527 (2005).
[6] A. Rousse, K. Ta Phuoc, R. Shah *et al.*, Phys. Rev. Lett. **93**, 135005 (2004).

[7]C. Rischel, A. Rousse, I. Uschmann, P. Albouy, J. Geindre, P. Audebert, J. Gauthier, E. Forster, J. Martin, and A. Antonetti, Nature (London) **390**, 490 (1997).
[8]T. M. Antonsen, Jr. and P. Mora, Phys. Rev. Lett. **69**, 2204 (1992).
[9]P. Sprangle, E. Esarey, J. Krall, and G. Joyce, Phys. Rev. Lett. **69**, 2200 (1992).
[10]N. E. Andreev, L. M. Gorbunov, V. I. Kirsanov, A. A. Pogosova, and R. R. Ramazashvili, JETP Lett. **55**, 571 (1992).
[11]J. M. Dawson, Phys. Rev. **133**, 383 (1959).
[12]J. Faure, Y. Glinec, A. Pukhov, S. Kiselev, S. Gordienko, E. Lefebvre, J.-P. Rousseau, F. Burgy, and V. Malka, Nature (London) **431**, 541 (2004).
[13]C. G. R. Geddes, C. Toth, J. van Tilborg, E. Esarey, C. B. Schroeder, D. Bruhwiler, C. Nieter, J. Cary, and W. P. Leemans, Nature (London) **431**, 538 (2004).
[14]S. P. D. Mangles, C. D. Murphy, Z. Najmudin *et al.*, Nature (London) **431**, 535 (2004).
[15]V. Malka, S. Fritzler, E. Lefebvre *et al.*, Science **298**, 1596 (2002).
[16]V. Malka, J. Faure, Y. Glinec, A. Pukhov, and J.-P. Rousseau, Phys. Plasmas **12**, 056702 (2005).
[17]A. Pukhov and J. Meyer-ter-Vehn, Appl. Phys. B: Lasers Opt. **74**, 355 (2002).
[18]M. Pittman, S. Ferre, J.-P. Rousseau, L. Notebaert, J.-P. Chambaret, and G. Cheriaux, Appl. Phys. B: Lasers Opt. **74**, 529 (2002).
[19]C. Ren, B. J. Duda, R. G. Hemker, W. B. Mori, T. Katsouleas, T. M. Antonsen, Jr., and P. Mora, Phys. Rev. E **63**, 026411 (2001).
[20]F. S. Tsung, C. Ren, L. O. Silva, W. B. Mori, and T. Katsouleas, Proc. Natl. Acad. Sci. U.S.A. **99**, 29 (2002).
[21]D. F. Gordon and B. Hafizi, Phys. Rev. Lett. **90**, 215001 (2003).
[22]W. B. Mori, IEEE J. Quantum Electron. **33**, 1942 (1997).
[23]C. E. Max, J. Arons, and A. B. Langdon, Phys. Rev. Lett. **33**, 209 (1974).
[24]G. Sun, E. Ott, Y. C. Lee, and P. Guzdar, Phys. Fluids **30**, 526 (1987).
[25]C. D. Decker, W. B. Mori, T. Katsouleas, and D. E. Hinkel, Phys. Plasmas **3**, 1360 (1996).
[26]O. Shorokhov, A. Pukhov, and I. Kostyukov, Phys. Rev. Lett. **91**, 265002 (2003).
[27]J. Faure, Y. Glinec, J. J. Santos, F. Ewald, J.-P. Rousseau, S. Kiselev, A. Pukhov, T. Hosokai, and V. Malka, Phys. Rev. Lett. **95**, 205003 (2005).
[28]J. A. Valdamis, G. Mourou, and C. W. Gabel, Appl. Phys. Lett. **41**, 211 (1982).
[29]Q. Wu and X.-C. Zhang, Appl. Phys. Lett. **67**, 3523 (1995).
[30]X. Yan, A. M. MacLeod, W. A. Gillespie, G. M. H. Knippels, D. Oepts, A. F. G. van der Meer, and W. Seidel, Phys. Rev. Lett. **85**, 3404 (2000).
[31]I. Wilke, A. M. MacLeod, W. A. Gillespie, G. Berden, G. M. H. Knippems, and A. F. G. van der Meer, Phys. Rev. Lett. **88**, 124801 (2002).
[32]M. L. Ter-Mikaelian, *High Energy Electromagnetic Processes in Condensed Mmedia* (Wiley-Interscience, New York, 1972).
[33]J. J. Santos, F. Amiranoff, S. D. Baton *et al.*, Phys. Rev. Lett. **89**, 025001 (2002).
[34]W. P. Leemans, C. G. R. Geddes, J. Faure *et al.*, Phys. Rev. Lett. **91**, 074802 (2003).
[35]J. van Tilborg, Phys. Rev. Lett. **96**, 014801 (2005).
[36]P. Kung, H.-C. Lihn, and H. Wiedmann, Phys. Rev. Lett. **73**, 967 (1994).
[37]U. Happek, A. J. Sievers, and E. B. Blum, Phys. Rev. Lett. **67**, 2962 (1991).
[38]S. D. Baton, J. J. Santos, F. Amiranoff *et al.*, Phys. Rev. Lett. **91**, 105001 (2003).
[39]W. P. Leemans, J. van Tilborg, J. Faure, C. G. R. Geddes, C. Tóth, C. B. Schroeder, E. Esarey, G. Fubiani, and G. Dugan, Phys. Plasmas **11**, 2899 (2004).
[40]J. Zheng, K. Tanaka, T. Miyakoshi, Y. Kitagawa, R. Kodama, T. Kurahashi, and T. Yamanaka, Phys. Plasmas **9**, 3610 (2002).
[41]C. Schroeder, E. Esarey, and J. van Tilborg, and W. P. Leemans, Phys. Rev. E **69**, 016501 (2004).